# Hyperspectral Imaging with Random Printed Mask

Yuanyuan Zhao Hui Guo Xun Cao Zhan Ma Tao Yue Xuemei Hu
School of Electronic Science and Engineering, Nanjing University

## Abstract

*Hyperspectral images can provide rich clues for various computer vision tasks. However, the requirements of professional and expensive hardware for capturing hyperspectral images impede its wide application. In this paper, based on a simple but not widely noticed phenomenon that the color printer can print color masks with a large number of independent spectral transmission responses, we propose a simple and low-budget scheme to capture the hyperspectral images with a random mask printed by the consumer-level color printer. Specifically, we notice that the printed dots with different colors stacked together, forming multiplicative, instead of additive, spectral transmission response, which therefore can generate new color filters with spectral transmission response uncorrelated with that of the original printer dyes. We validate the corollary by both the simulated and real captured data, and based on it, we propose a simple snapshot hyperspectral camera. A convolutional neural network (CNN) based method is developed to reconstruct the hyperspectral images from the captured image. The effectiveness and accuracy of the proposed system are verified on both synthetic and real captured images.*

## 1. Introduction

Spectra can provide additional information of scenes beyond the ability of human eyes and commercial RGB cameras, having great potential to facilitate computer vision tasks [3, 9, 28]. However, the high complexity and cost of spectral imaging systems greatly raise the difficulty of acquiring spectral images, and thus limit the wide application of spectral information.

Traditionally, to capture a spectral image, which is a 3D data cube with spatial and spectral dimensions, the scanning based methods (either the spatial scanning[17] or the spectral scanning[15]) are required. These scanning based system can capture images with several to hundreds spectral channels, sacrificing the ability to handle dynamic scenes. To take the spectral image in a single snapshot, the snapshot spectral imaging methods are proposed in the past few years [6, 10, 16, 24, 30, 31]. However, most of these systems suffer from the system complexity, which is difficult to calibrate. Customized spectral filter based methods are also proposed to realize compact hyperspectral imaging [5, 19, 22, 27], while these method requires customized color filter of high-precision fabrication process. RGB cameras are also studied to be turned into spectrometers [2, 4, 26, 23, 32], while the uncorrelated spectral transmission number is limited, which is not enough to resolve complex spectral details.

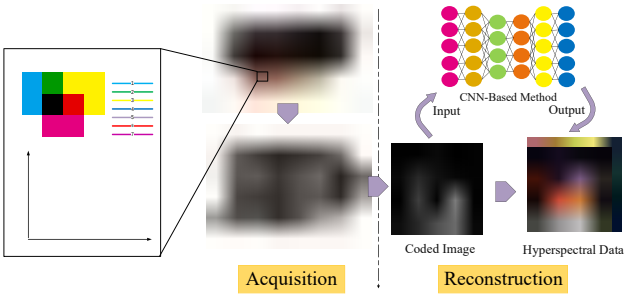


Figure 1. Overview of the proposed hyperspectral imaging system: with a consumer-level printer, a random color printed mask can be attached to the sensor of the camera to sample the hyperspectal images. Through randomly overlaying ink droplet, the spectral transmission response of different points is rendered high uncorrelated and faciliate the full spectrum recovery with details. A convolutional neural network is proposed to recover the hyperspectral images from the randomly coded images.

In this paper, we propose a simple and low-cost spectral imaging scheme with a color mask, which can be printed by consumer-level printers. The idea of the proposed system is based on a simple but not widely noticed phenomenon, i.e. the spectral transmission response of overlappingly printed color dots is the multiplication of the spectral transmission response of each overlapped color dots. The multiplied spectral transmission response is linearly uncorrelated with that of the printer inks. Therefore, we can generate a large number of uncorrelated spectral transmission response using few kinds of printer inks. Benefiting from these uncorrelated responses, our scheme can provide much more well-conditioned sensing model for hyperspectral imaging scenario. The proposed method are validated on both the simulated and real data, and a simple prototype of snapshot

hyperspectral camera is built. We demonstrate that hyperspectral images can be reconstructed well with high quality by a CNN-based neural network from observations of proposed system. The main contributions of the paper are:

- We *propose* to generate a large number of uncorrelated spectral transmission response of mask by using consumer-level color printers and *p*ropose a simple spectral imaging scheme based on the randomly printed color mask.
- We *develop* a CNN-based reconstruction network to recover the hyperspectral images from observations.
- We *build* a prototype imaging system to verify this approach and *demonstrate* the feasibility and effectiveness on both synthetic and experimental data.

## 2. Related Work

Snapshot hyperspectral imaging technologies has been evolving rapidly in the last few decades. To capturing the 3D hyperspectral images with 2D imaging sensor in a snapshot way, either spatial or spectral coding are introduced. In terms of the specific coding techniques, existing methods can be divided into three main categories: dispersion based spectral imaging methods [6, 16, 24, 30, 31], the scattering based spectral imaging methods [12, 29], and the spectral filter based methods [2, 4, 5, 13, 19, 22, 23, 26, 27, 32].

**Dispersion based Spectral Imaging Methods**. With dispersive elements, e.g. prisms or gratings, the spectrum of each point is spread spatially. Through introducing a spatial coding, the spectral information is coded indirectly and captured [6, 10, 16, 24, 30, 31]. While these spectral imaging method could realize snapshot and high quality hyperspectral imaging, sophisticated calibration are always required and the system is bulky. Compared with these methods, our hyperspectral imaging method only requires to print a color mask and attach the color mask in front of the camera sensor, which is easy to implement and of low cost, promising for wider application in practice.

**Scattering based Spectral Imaging Methods**. Besides spectral coding through introducing dispersers, scattering medium is also introduced to encode the spectral information with different speckle patterns [12, 29]. Hyperspectral images could be recovered through deblurring with the precalibrated speckle pattern. While these method are promising for compact hyperspectral imaging, the spectral resolving ability is largely limited due to the speckle correlation among different wavelengths. In our method, we propose to use overlaying of ink drops to generate spectral modulations which is highly uncorrelated and could enable high quality encoding of hyperspectral imaging.

**Spectral Filter based Spectral Imaging Methods**. Other than those indirect spectral coding methods, spectral imaging could also be realized through direct spectral coding: designing and attaching the spectral filter in front of the camera sensor [5, 19, 22, 27]. Deep learning or dictionary learning based methods, which exploit the sophisticated spatial-spectral prior, are proposed for high quality hyperspectral recovery [8, 13, 14]. These hyperspectral imaging methods may require high precision manufacturing of spectral filters, while our spectral imaging method only requires to print a color mask with a consumer-level printer.

Recently, turning commercial RGB cameras into hyperspectral imaging also emerged as a hot research topic [2, 4, 23, 26, 32], which is promising for a low-cost spectrometer. However, the uncorrelated spectral modulations are limited and may not be enough to recover spectral details. Our method could provide various uncorrelated spectral modulations, making it possible to realize higher quality encoding and recovery of hyperspectral information.

In all, we propose a novel low-cost and easy-to-implement hyperspectral imaging technique. The calibration of our method is easy and most importantly, through exploiting the new generated spectral transmission responses of randomly overlaying ink drops, detailed hyperspectral information could be encoded. We propose a CNN-based network model to extract the hyperspectral images and demonstrate the effectiveness of our method through both synthetic and physical experiments.

## 3. Multiplicative Character of Spectral Transmission Responses

The basis of our work is that the spectral transmission response of inks of different colors is various and the spectral information can be encoded with randomly printed color films. We investigate the printed color dot characteristics, formulate the mask printing model and analyze the color transmission responses with different printing parameters. Based on the analysis, we could choose the optimal physical parameters to print our spectral coding mask.

### 3.1. Characteristic Exploration of Single Color Dot

*Random distribution Characteristics*. We first observe the distribution of ink droplets at the micron level using a microscope with 20X magnification. The CMYK color mode, commonly used in color printing, contains four standard colors, i.e. cyan (C), magenta (M), yellow (Y), and black (K). Since black ink absorbs light of all wavelengths, we generated a background picture with CMYK mode in which case C, M and Y channels is set to 10 respectively and K channel is set to 0. We print a uniform mask with the CMYK value on a transparent film and observed the printed picture under the microscope, as shown in Fig. 2(a). It can be observed that the positions of droplets at the micron level are not regularly arranged, but relatively random and uncontrolled. Each individual drop of ink is approximately round.

Figure 2. (a) Image of ink droplet distribution at micron level. (b) Spectral transmission response of CMY color printed film.

New colors such as purple, green and orange are produced due to the overlapping of the CMY ink droplets.

*Multiplicative Stacking Characteristics*. Observing the random distribution of ink drops, we further more explore how would the spectral transmission response change if different ink droplets are stacked. We assume that the transmission response would be a multiplication of the transmission response of each overlapped ink droplet, which can be formulated as

$$\mathbf{c}_p = \prod_i \mathbf{c}_i, \tag{1}$$

where $\mathbf{c}_p$ means the transmission response of overlapped layers and $\mathbf{c}_i$ is the transmission response of the $i$ th layer.

We conduct an experiment to verify the assumed stacking model. A single point spectrometer (ASD TerraSpec 4 Standard-Res Mineral Analyzer) is used to measure the transmission responses. After removing the influence of light source and camera spectral sensitivity response, the transmission responses of CMY inks are shown in Fig. 2(b). We calculate the transmission response of the overlapped ink droplets of magenta- magenta and cyan-magenta and measure that with the single spectrometer. As shown in Fig. 3, the measured transmission responses match well with the calculated one by multiplication.

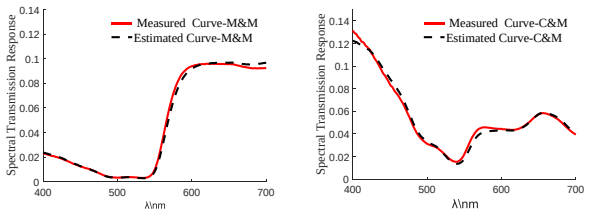


(a) (b)

Figure 3. (a) Transmission response with the same ink stacking. (b) Transmission response with different ink stacking. The estimated spectral transmission responses are calculated by Eq. (1).

### 3.2. Modeling Multilayer Monochromatic Mask

With the multiplicative stacking model, we proceed to model the multilayer monochromatic mask to simulate the transmission response matrix of printed mask. The main factors to be considered in modeling are ink density $p$, number of layers $L$, diameter of single droplet $d$ and number of ink colors. For one monochromatic layer, the printed mask can be formulated as

$$\mathbf{M}_i = \mathbf{I}(p) * \mathbf{K}(d, \mathbf{c}_i), \tag{2}$$

where $\mathbf{I}(p)$ denotes the random 0-1 printing pattern of dimension $H \times W$. $\mathbf{M}_i$ means the mask transmission response matrix, $K$ denotes the circle kernel whose diameter is $d$ (the shape of printed drop is approximately circular in practice). $\mathbf{c}_i$ is the spectral transmission response of the $i$ th layer. $*$ means the convolutional operation.

For a mask of mixed colors, it is equivalent to print multiple layers of various colors. Inspired by the multiplicative stacking characteristics, multilayer monochromatic mask $M$ can be modeled as

$$\mathbf{M} = \prod_{i=1}^{L} \mathbf{M}_i, \tag{3}$$

where $\prod$ means element-wise product.

According to the established model, we simulate the mask printed under different conditions and discuss the effects of these parameters on spectral modulation to select the best print settings for spectral reconstruction in the next section.

### 3.3. Characteristic Exploration of Multilayer Monochromatic Mask

In this chapter, we analyze the spectral reconstruction perfomance of different physical parameters for printing the color mask and choose the optimal one for our imaging technique. Based on the spatial consistency hypothesis of spectral data in natural scenes, the imaging model of the light reflected by objects in the scene through printed mask can be expressed as

$$\mathbf{y} = \mathbf{C}\mathbf{s}, \tag{4}$$

where $\mathbf{y} = [y_1, y_2, \cdots, y_n]^T$ is signal encoded by printed mask, $\mathbf{C} = [\mathbf{c}_1, \mathbf{c}_2, \cdots, \mathbf{c}_n]^T$ refers to transmission responses of printed mask, and $\mathbf{s}$ means spectra of the scene. Figure(5) shows a pseudo-color image of the print mask under several parameters.

As for printing the color mask, there are four physical parameters: the diameter of each ink droplet, the print density, the color number and the overlapping layer number. To choose the parameter value, we firstly synthesize the color mask with different color number and layer number and the other parameters remain consistent, as shown in Figs. 4(a)-(b), we plot the rank of the transmission response of the mask and the corresponding reconstruction result corresponding to different parameters. As shown in Fig. 4(a),

Figure 4. Setting ink density $p$ to 0.01 and ink droplet diameter $d$ to 4 pixels: (a) rank analysis for different number of colors used, (b) reconstructed spectrum at parameter marked in (a). Setting ink droplet diameter $d$ to 4 pixels and color number to 10: (c) rank analysis for different layers and density, (d) reconstructed spectrum at parameter marked in (c). Setting ink density $p$ to 0.01 and color number to 10: (e) rank analysis for different droplet diameter, (f) reconstructed spectrums at parameter marked in (e).

the rank of the transmission response of the printed mask increases with the overlapping layer number. The rank of more colors is larger than that with smaller color number, we show the reconstruction results of a spectrum with different physical parameters, as marked in Fig. 4(a). We can see that with the same overlapping number, the more color number, the rank of the transmission response is higher and the ground truth spectrum is reconstructed with higher fidelity. Print density also plays a key role in mask transmission response characteristics. As shown in Figs. 4(c)-(d), when the print density is 0.001 or 0.01, the rank and hyperspectral reconstruction results increases as the number of overlapping layers increases. However, when the print density is 0.1, the rank and the reconstruction result goes down as the overlapping layer number increases. High density would decrease the light throughput and deteriorate the spectral coding ability of the color mask. We finally analyze the effect of the diameter size. The changing trend of rank is shown in the Figs. 4(e)-(f). It can be inferred that the

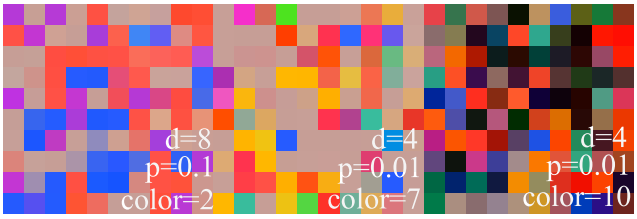


Figure 5. The image of the color mask with different parameters.

larger diameter size, the more information will be collected when coding in the case of relatively fewer printing layers. However, when the diameter is too large (8 pixels), printing more layers will lead to a decrease in randomness. Some of the simulated print masks are shown in Fig. 5, ink droplets of different colors are randomly printed and overlap with each other randomly, generating highly uncorrelated spectral transmission responses.

In our experiments, considering the trade off between the light throughput and the recovering ability of the color mask, we choose the print density to be 0.01, diameter 4, color 7 and the layer number 14 as our final physical parameter for the printing of the color mask. In the next section, we will develop a CNN for the reconstruction of hyperspectral image with our imaging technique.

## 4. Image Formation Model and Inverse Method

By placing the color mask in front of the sensor, the spectral images are spectrally encoded, integrated along wavelength and captured by a 2D sensor. The image formation model is

$$\mathbf{I}(x,y) = \sum_{\lambda} \mathbf{\Phi}(x,y,\lambda)\mathbf{S}(x,y,\lambda), \tag{5}$$

where $\Phi$ denotes the spectral transmission matrix of the color mask, $\mathbf{S}$ denotes the 3D hyperspectral images, and $\mathbf{I}$ is the captured image. Reconstructing the 3D hyperspectral images $\mathbf{S}$ from the captured 2D coded image is highly underdetermined, where sophisticated sparsity prior of hyperspectral images is required. Dictionary based methods has been pioneeringly applied to introduce the statistical prior of hyperspectral images into the inverse problem and successfully recover high quality hyperspectral images [1, 14, 24]. Beyond that, CNN which is expert in learning statistical priors from data, have also been applied and achieved remarkable performance in hyperspectral image reconstruction [8, 13, 23].

In this paper, we propose a CNN-based neural network for the spectral reconstruction. In order to increase the receptive field (RF [20]) of the model and enable it to integrate the coded information of mask of different size level, a multiscale network model is employed. The network structure is shown in Fig. 6. The proposed method learns an

end-to-end mapping from a large number of coded image and ground truth hyperspectral image pairs. The input of network is a two-dimensional image encoded by printing mask, and the output the is reconstructed spectral image. The CNN-based model we used is represented as $\mathcal{F}$. The input and output pairs fed to $\mathcal{F}$ is represented as $\{\mathbf{I}_i|\mathbf{S}_i\}_1^N$. $\mathbf{I}$ is obtained by Eq.(5) in synthetic experiment with ground truth hyperspectral images $\mathbf{S}$, where $\Phi$ means the transmission response matrix of the color mask, $\Phi \in R^{H\times W\times \Lambda}$ and $\mathbf{S} \in R^{H\times W\times \Lambda}$, $\Lambda$ is the spectral dimension. The network output is

$$\hat{\mathbf{S}} = \mathcal{F}(\mathbf{I}). \tag{6}$$

**Network structure**. Our model (Fig.6) is based on the multiscale structure, which is downsampled three times with maximum pooling. The size of feature maps is shrunk to half of previous layer after downsampling. Bilinear upsampling instead of deconvolution operation is used to prevent the checkboard effect. Bottleneck in Resnet [18] is added following upsampling to smooth the feature map. Skipping connection are introduced in our network structure to combine the shallow information and deep feature domain. The multiscale scheme is proposed basically on the purpose to extract the correlation information from pixels in different scales of receptive fields for better spectral reconstruction.

**Loss function**. Parameters of each layer in $\mathcal{F}$ is defined as $\theta = \{\mathbf{W}_l, \mathbf{b}_l\}_1^{d+1}$, and $d$ is the number of hidden layers. These parameters are trained with the loss function in Eq. 7. The first term is the mean squared error (MSE) of the groundtruth hyperspectral image $\mathbf{S}$ and the predicted hyperspectral image $\hat{\mathbf{S}}$ from the network. In order to recover the detailed characteristic information in spectral dimension, we proposed the spectrum constancy loss as the second term in Eq. 7, which constraints the first-order derivative of $\mathbf{S}$ and $\hat{\mathbf{S}}$ to be similar. In addition, decay term of weights is included to avoid overfitting.

$$\begin{aligned} L = &\underbrace{\beta_1\|\mathcal{F}(\mathbf{I}) - \mathbf{S}\|_2^2}_{\text{data term}} + \underbrace{\beta_2\|\bigtriangledown_\lambda \hat{\mathbf{S}} - \bigtriangledown_\lambda \mathbf{S}\|^2}_{\text{spectrum constancy loss}} \\ &+ \underbrace{\frac{\tau_w}{2}\sum_1^{d+1}\|\mathbf{W}_l\|^2}_{\text{decay term}} \end{aligned} \tag{7}$$

**Implementation Details**. The databases used for training are publicly available including Harvard [7], Columbia [33], KAIST [8], and Manchester [25, 11] spectral image database. Data augmentation method is used to preprocess datasets by means of cutting, scaling, rotation, etc. 40000 enhanced data pairs of size $256\times256\times31$ are sampled. The augmented dataset is divided into training and validation set by $4:1$. Pytorch framework is employed to train our model. ADAM [21] gradient descent method is used. The leaning rate is set at $10^{-4}$ at the beginning, and is scaled to $1/3$ of previous one starting from the 6th epoch. $\beta_2$ is gradually increased from the 6 th epoch, scaled by 1.1 times each epoch. The weight $\tau_w$ for the decay term is set to $10^{-8}$. With 11 hidden layers, the network training process lasted about 24 hours. The hardware platform we used is configured with an Intel(R) CPU E5-2609 with 64GB memory and NVIDIA Tesla P100 with 16GB of memory. Zero mean simulated Gaussian noise with a standard deviation of 5 is added during training and testing.

## 5. Experiment

We demonstrate the effectiveness of our method through simulation and physical experiments. In simulation, we compare our spectral reconstruction with other three typical methods [16, 24, 26], both quantitatively and qualitatively. Our method performs highest quality spectral reconstruction compared with the other methods. In physical experiments, we build a prototype system, capture the data with our imaging system, and recover the spectral response of the scene, we demonstrate our method through comparing the recovered spectra of points by our method with the spectra captured with the ASD spectrometer .

### 5.1. Experiments on Synthetic Spectral Data

We first carry out experiments on synthetic data to verify that the coding method of our system can collect more information of the spatial and spectral data. Existing reconstruction techniques share an intrinsic trade-off between spectral accuracy and spatial resolution, however our coding method provides abundant unrelated observation bases that can recover spectral details. Coded information is restored based on data-driven reconstruction method. We compare our reconstruction method against other three state-of-the-art methods: training-based method from single RGB image (Rgb) [26], dictionary-learning-based sparse coding (SC) [24], and compressive spectral imaging with CASSI-based dual-disperser architecture (DC) [16]. For fair comparison, parameters of the three methods are traversed and set to be the ones with the best performance.

**Quantitative Comparisons of Reconstruction**. As shown in Fig. 7, we test our proposed method on four validation datasets which respectively are Harvard [7], Columbia [33], KAIST [8], Manchester [11, 25] spectral dataset. Average peak signal to noise ratio (PSNR), structure similarity index metrics (SSIM), mean squared error (MSE), and time to reconstruct hyperspectral images with $256\times256\times31$ data cube resolution are presented. Our reconstruction method outperforms all three methods in all terms of these objective metrics, the PSNR and SSIM of our results are at least 8.31dB and 0.07 higher and the MSE of our methods is much lower than the other methods. In terms of reconstruction speed, the time required by our method is orders of

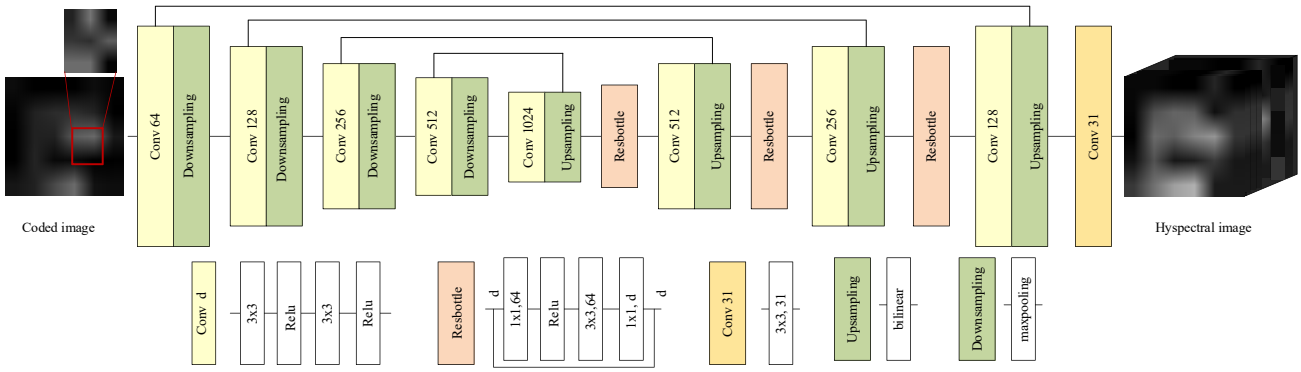


Figure 6. CNN-based network structure. The input an spectrally coded RGB images by our color printed mask, and the output is the predicted hyperspectral images of 31 channels. The multiscale network is composed of convolution layers, bilinear upsampling, maxpooling and Resbottle modules, which can exploit correaltion among pixels over receptive fields of different scales with an elegantly amount of parameters.

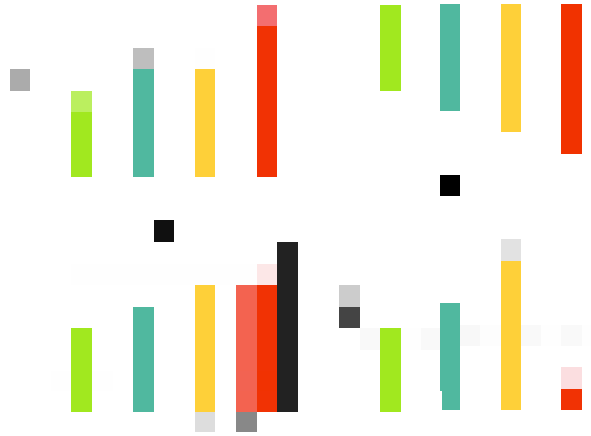

Figure 7. Objective metrics comparison: average PSNR, SSIM, MSE, and required reconstruction time of different methods over the four database (Manchester, Columbia, Harvard, KAIST) are compared with our methods, quantitatively demonstrate our method.

magnitude shorter than the other three methods. The effectiveness of our method is demonstrated quantitatively upon hyperspectral databases.

**Qualitative Comparisons of Reconstruction**. Furthermore, we show the reconstruction of our method and the other three method on four images, each from a different database. To compare the results clearly, we first calculate the corresponding RGB images with the reconstructed hyperspectral images and RGB spectral response of commercial RGB cameras, as the 1 4 rows in Fig. 8. Through comparing with the other methods, the color image calculate from the hyperspectral images recovered with our method is the most similar with the ground truth. This could be further demonstrate while comparing the error maps of RGB images of different methods, in the 5 8 the row. We pick four point from these four scene and compare the recovered spectrum directly in the first column, 5 8 rows. As is shown, our methods could recover most of the details of the spectrum, demonstrating the effectiveness of spectral coding.

### 5.2. Experiments on Real Captured Data

To further prove the validity of our spectral acquisition method, we build a prototype system with the printed mask. To make the mask more qualified and random, we firstly investigate the transmission curves of 10 inks in the market, and compare the cross correlation coefficient between them. Seven inks which is least relevant with each other is selected and randomly printed on the transparent film by printer. According to the analysis above, diameters between 4 and 8 pixels is better. A mask is produced by printing about 14 layers when the droplet density was set to 1%. Since removing the protective glass in front of the sensor and stick the printer color mask to the sensor may needs sophisticated manufacturing or fabrication technique to avoid potential artifacts, here we leave that engineering part for future work and build a relay system to simply demonstrate our method.

As shown in Fig. 10, the acquisition system we propose includes objective lens, printed mask, relay lens and the imaging sensor. Objective lens is used to focus the light from the scene on the printed mask, spectral information is modulated by the printed mask. The modulated light is finally imaged by the sensor through the relay lens.

The spectral transmission response of the printed mask is calibrated using a high resolution spectrophotometer (with spectral resolution: 0.1nm ). We change the emission wavelength of the spectrophotometer and direct the monochromatic light into the integrating sphere to produce a spatially uniform light. The transmitted images are captured every

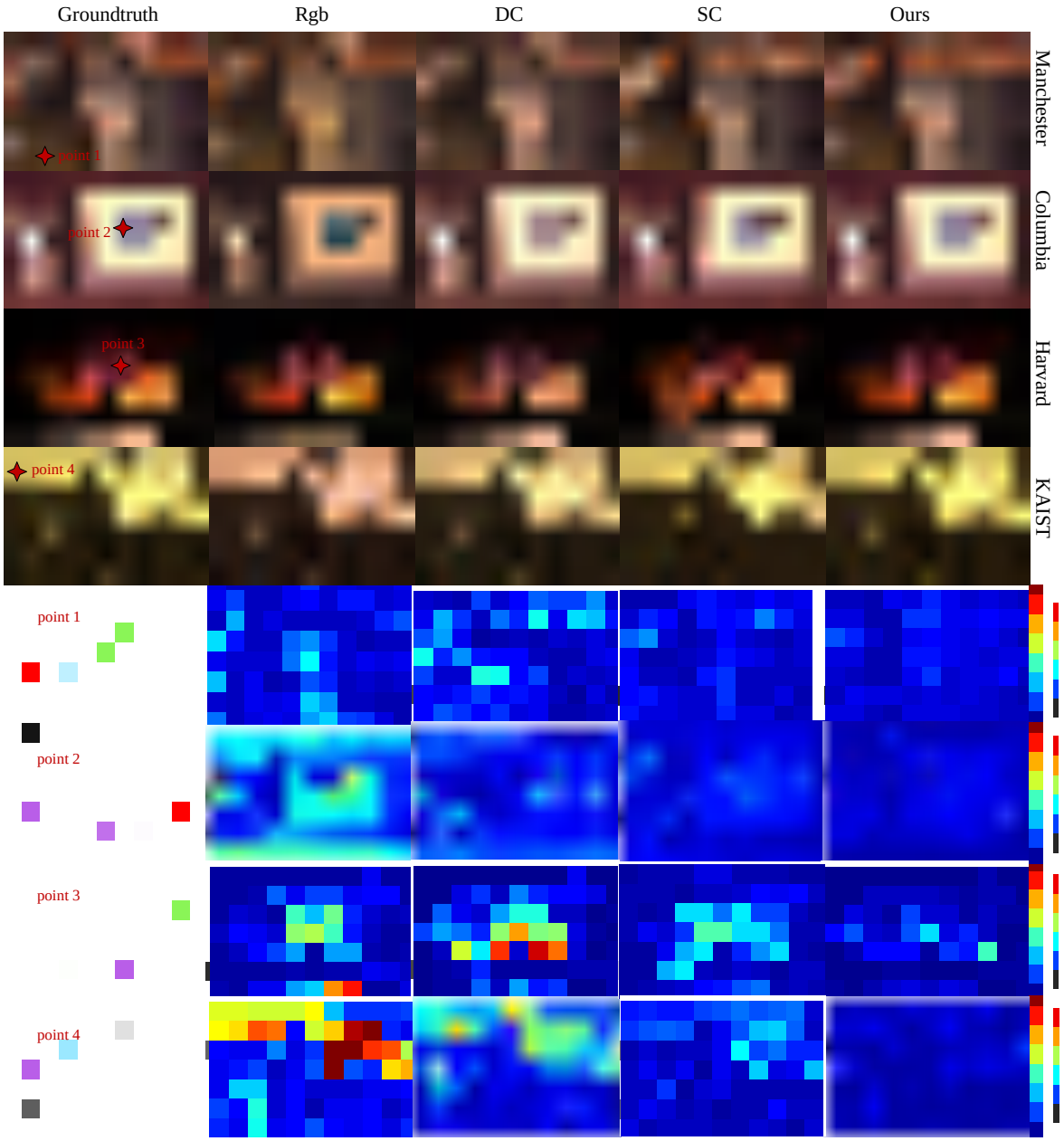


Figure 8. Simulation results on four images, each from a hyperspectral database (Manchester, Columbia, Harvard, KAIST). We compare the synthetic RGB images and the spectrum at different points with the other three methods. Error map are also provided to compare the reconstruction accuracy of different methods.

10 nm from 400 nm to 700 nm, which is the spectral transmission response. Fig. 10 shows the transmitted image at different bands. The spectrum of some of the points are also shown in Fig. 10.

We use the calibrated transmission spectral response and the hyperspectral image database to generate 40000 training data pairs of size $256 \times 256 \times 31$. It took approximately 24 hours to training the network. Zero mean simulated Gaussian noise with a standard deviation of 5 is added during training and testing the same as synthetic experiment.

We capture the spectrally coded image with the prototype system and recovered the hyperspectral image with the trained network. We only need to calibrate the acquisition system once to get the spectral transmission response $\mathbf{\Phi}$. Under the irradiation condition of iodine tungsten lamp light source, we collect several coded images as shown in the first column in Fig. 9. The results are shown in Fig. 9. The first column is the captured image of different scenes.

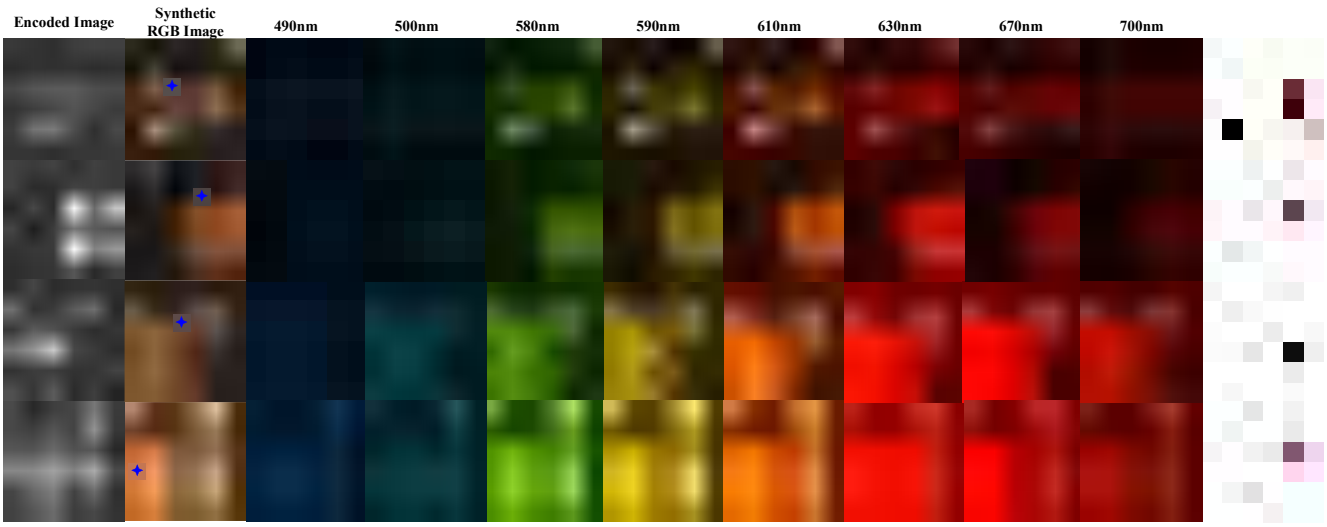


Figure 9. Experimental results of different scenes, the first column is the captured coded image, the second column is the synthetic RGB image with the recovered spectrum, the 3-10 th column is the recovered hyperspectral channels, the last row is the comparison between the recovered spectrum with the spectrum captured by a ASD spectrometer.

The second column is the synthetic RGB image with the recovered hyperspectral images. The 3-10 th column are the single band spectral images of 490 nm, 500 nm, 580 nm, 590 nm, 610 nm, 630 nm, 670 nm and 700 nm.

To verify the effectiveness of our method, we capture the spectrum with a ASD spectrometer and compare the reconstructed spectrum with the spectrum captured with a ASD spectrometer. We use the high reflectivity whiteboard to correct the response differences between ASD and the sensor we use. As shown in the last column at blue points, our method could recover most of the spectral details. In all, through the physical experiments, we demonstrate that through combing the random color spectral encoding and CNN-based decoding, our method could realize high quality hyperspectral imaging.

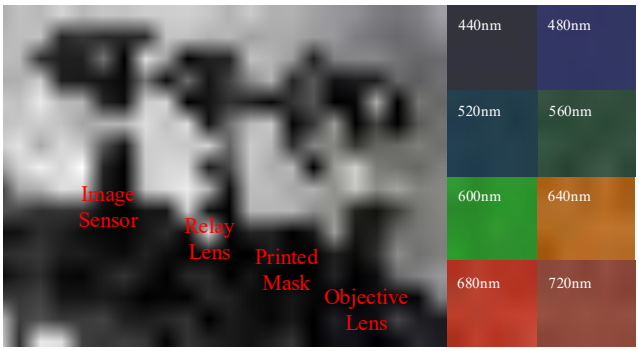


Figure 10. Prototype hyperspectral imaging system and the captured transmitted images at different wavelengths for calibration.

## 6. Conclusion

In this paper, we propose a simple, low-budget and fast hyperspectral imaging methods. We observe that the transmission spectrum of overlappingly printed color mask is the multiplication of the spectral transmission response of each layer, which could introduce a large number of a large number of independent spectral transmissions. Through printing multilayer random color pattern, we could get an efficient spectral coding color mask. Combined with the novel spectral coding color mask, we develope a CNN-based network model to recover the hyperspectral information from the coded image with our color mask. Our hyperspectral imaging is of the state-of-the art spectral retrieving quality and the orders of magnitude faster speed of our hyperspectral reconstruction enables wider applications under dynamic high level tasks based on hyperspectral images [3, 28].

Future work would be developing a compact spectrometer based on our method. Although our prototype system is not compact in its current relay-system implementation, our method is indeed promising for a compact hyperspectral imager through fabricating the spectral mask upon the sensor, just as most of the spectral coding based spectrometer [5, 19, 22].

## Acknowledgments

We would like to acknowledge funding from NSFC Projects 61671236, and National Science Foundation for Young Scholar of Jiangsu Province, China (Grant No. BK20160634), and Fundamental Research Funds for the Central Universities, China (Grant No. 0210-14380047).

## References


[1] B. Arad and O. Ben-Shahar. Sparse recovery of hyperspectral signal from natural rgb images. In *Proc. ECCV*, pages 19–34. Springer, 2016. 4324

[2] B. Arad and O. Ben-Shahar. Filter selection for hyperspectral estimation. In *Proc. CVPR*, pages 21–26, 2017. 4321, 4322

[3] V. Backman, M. B. Wallace, L. Perelman, J. Arendt, R. Gurjar, M. Müller, Q. Zhang, G. Zonios, E. Kline, T. McGillican, et al. Detection of preinvasive cancer cells. *Nature*, 406(6791):35, 2000. 4321, 4328

[4] S.-H. Baek, I. Kim, D. Gutierrez, and M. H. Kim. Compact single-shot hyperspectral imaging using a prism. *ACM Trans. on Graph. (TOG)*, 36(6):217, 2017. 4321, 4322

[5] J. Bao and M. G. Bawendi. A colloidal quantum dot spectrometer. *Nature*, 523(7558):67, 2015. 4321, 4322, 4328

[6] X. Cao, H. Du, X. Tong, Q. Dai, and S. Lin. A prism-mask system for multispectral video acquisition. *IEEE Trans. Pattern Anal. Mach. Intell.*, 33(12):2423–2435, 2011. 4321, 4322

[7] A. Chakrabarti and T. Zickler. Statistics of Real-World Hyperspectral Images. In *Proc. CVPR*, pages 193–200, 2011. 4325

[8] I. Choi, D. S. Jeon, G. Nam, D. Gutierrez, and M. H. Kim. High-quality hyperspectral reconstruction using a spectral prior. *ACM Trans. on Graph. (TOG)*, 36(6):218, 2017. 4322, 4324, 4325

[9] W. Debskia, P. Walczykowskia, A. Klewskia, and M. Zyznowskib. Analysis of usage of multispectral video technique for distinguishing objects in real time. In *20th ISPRS*, 2004. 4321

[10] M. Descour and E. Dereniak. Computed-tomography imaging spectrometer: experimental calibration and reconstruction results. *Appl. Opt.*, 34(22):4817–4826, 1995. 4321, 4322

[11] D. H. Foster, K. Amano, S. M. Nascimento, and M. J. Foster. Frequency of metamerism in natural scenes. *JOSA A*, 23(10):2359–2372, 2006. 4325

[12] R. French, S. Gigan, and O. L. Muskens. Speckle-based hyperspectral imaging combining multiple scattering and compressive sensing in nanowire mats. *Opt. Lett.*, 42(9):1820–1823, 2017. 4322

[13] Y. Fu, T. Zhang, Y. Zheng, D. Zhang, and H. Huang. Joint camera spectral sensitivity selection and hyperspectral image recovery. In *Proc. ECCV*, pages 812–828. Springer, 2018. 4322, 4324

[14] Y. Fu, Y. Zheng, I. Sato, and Y. Sato. Exploiting spectral-spatial correlation for coded hyperspectral image restoration. In *Proc. CVPR*, pages 3727–3736, 2016. 4322, 4324

[15] N. Gat. Imaging spectroscopy using tunable filters: a review. In *Wave. Appl. VII*, volume 4056, pages 50–65. International Society for Optics and Photonics, 2000. 4321

[16] M. Gehm, R. John, D. Brady, R. Willett, and T. Schulz. Single-shot compressive spectral imaging with a dual-disperser architecture. *Opt. Express*, 15(21):14013–14027, 2007. 4321, 4322, 4325

[17] R. O. Green, M. L. Eastwood, C. M. Sarture, T. G. Chrien, M. Aronsson, B. J. Chippendale, J. A. Faust, B. E. Pavri, C. J. Chovit, M. Solis, et al. Imaging spectroscopy and the airborne visible/infrared imaging spectrometer (aviris). *Remote Sens.S of Env.*, 65(3):227–248, 1998. 4321

[18] K. He, X. Zhang, S. Ren, and J. Sun. Deep residual learning for image recognition. In *Proc. CVPR*, pages 770–778, 2016. 4325

[19] J. Jia, K. J. Barnard, and K. Hirakawa. Fourier spectral filter array for optimal multispectral imaging. *IEEE Trans. Pattern Anal. Mach. Intell.*, 25(4):1530–1543, 2016. 4321, 4322, 4328

[20] E. R. Kandel, J. H. Schwartz, T. M. Jessell, D. of Biochemistry, M. B. T. Jessell, S. Siegelbaum, and A. Hudspeth. *Principles of neural science*, volume 4. McGraw-hill New York, 2000. 4324

[21] D. P. Kingma and J. Ba. Adam: A method for stochastic optimization. *arXiv preprint arXiv:1412.6980*, 2014. 4325

[22] P.-J. Lapray, X. Wang, J.-B. Thomas, and P. Gouton. Multispectral filter arrays: Recent advances and practical implementation. *Sensors*, 14(11):21626–21659, 2014. 4321, 4322, 4328

[23] H. Li, Z. Xiong, Z. Shi, L. Wang, D. Liu, and F. Wu. Hsvcnn: Cnn-based hyperspectral reconstruction from rgb videos. In *Proc. ICIP*, pages 3323–3327. IEEE, 2018. 4321, 4322, 4324

[24] X. Lin, Y. Liu, J. Wu, and Q. Dai. Spatial-spectral encoded compressive hyperspectral imaging. *ACM Trans. on Graph. (TOG)*, 33(6):233, 2014. 4321, 4322, 4324, 4325

[25] S. M. Nascimento, F. P. Ferreira, and D. H. Foster. Statistics of spatial cone-excitation ratios in natural scenes. *JOSA A*, 19(8):1484–1490, 2002. 4325

[26] R. M. Nguyen, D. K. Prasad, and M. S. Brown. Training-based spectral reconstruction from a single rgb image. In *Proc. ECCV*, pages 186–201. Springer, 2014. 4321, 4322, 4325

[27] S. Nie, L. Gu, Y. Zheng, A. Lam, N. Ono, and I. Sato. Deeply learned filter response functions for hyperspectral reconstruction. In *Proc. CVPR*, pages 4767–4776, 2018. 4321, 4322

[28] Z. Pan, G. Healey, M. Prasad, and B. Tromberg. Face recognition in hyperspectral images. *IEEE Trans. Pattern Anal. Mach. Intell.*, 25(12):1552–1560, 2003. 4321, 4328

[29] S. K. Sahoo, D. Tang, and C. Dang. Single-shot multispectral imaging with a monochromatic camera. *Optica*, 4(10):1209–1213, 2017. 4322

[30] A. Wagadarikar, R. John, R. Willett, and D. Brady. Single disperser design for coded aperture snapshot spectral imaging. *App. Opt.*, 47(10):B44–B51, 2008. 4321, 4322

[31] L. Wang, Z. Xiong, D. Gao, G. Shi, W. Zeng, and F. Wu. High-speed hyperspectral video acquisition with a dual-camera architecture. In *CVPR*, pages 4942–4950, 2015. 4321, 4322

[32] S. Wug Oh, M. S. Brown, M. Pollefeys, and S. Joo Kim. Do it yourself hyperspectral imaging with everyday digital cameras. In *Proc. CVPR*, pages 2461–2469, 2016. 4321, 4322

[33] F. Yasuma, T. Mitsunaga, D. Iso, and S. K. Nayar. Generalized assorted pixel camera: postcapture control of resolution, dynamic range, and spectrum. *IEEE Trans. on Imag. Proc.*, 19(9):2241–2253, 2010. 4325